Anisotropic Contraction in a Magnetically Hard but Mechanically Ultra-Soft Foam for Precise Drug Delivery

Zisheng Zong, Shuo Zhang, and Zhigang Wu*

Hard magnetic soft materials (HMSMS) have been recently intensively explored in soft robots, owing to its native advantages such as untethered, rapid and reversible actuation, as well as large shape changes. However, in the existing studies, HMSMS is majorly applied by a magnetic field to produce bending, folding, and even twisting, that is, shape morphing, to realize multimodal locomotion. Meanwhile, such as contraction deformation, which may be employed in precise drug delivery, has been neglected in a long term. Here, an anisotropic contraction in a porous structure, hard magnetic foam (HMF), which is mechanically ultra-soft (with a shear modulus of 4.5 kPa) but magnetically hard (with a residual magnetic flux density of 12 mT), is reported. The investigation of HMF structures indicates that anisotropic contraction is dominated by the magnetodeformational effect and the magnetic body-force against support constraint. By adjusting the magnetic fields directions, the relationship between these two factors can be regulated to achieve a maximum contraction of 43% (synergy) or negligible deformation (antagonism). Finally, HMF is utilized to realize precision drug delivery since it has the advantages of no leakage during moving, precisely adjustable drug release rate (from 0.008 to 0.62 mL min^{-1}), and no residues after leaving.

1. Introduction

Being capable of responding to various external stimuli such as light, heat, electricity, and magnetic fields, a new class of soft materials, stimuli-responsive soft materials, is emerging.[1–4] Among them, of particular, magnetic-responsive soft materials have obtained considerable advancements in the design, modeling, and fabrication processes, resulting in broadening their application boundaries.[5] Magnetic-responsive soft materials, in general, are fabricated by embedding ferromagnetic particles into a soft matrix.[6–9] Based on the magnetization characteristics (mainly, coercivity) of magnetic fillers, magnetic-responsive soft materials can be classified into three

categories: soft magnetic, hard magnetic, and superparamagnetic soft materials.[5] Of particular, hard magnetic soft materials (HMSMS) have been widely used in soft robotics, flexible electronics, and biomedicine, which provide quite a few unique benefits: first, quick response to remote external magnetic stimuli (i.e., fast actuation); second, structures with predefined programmable functionalities to perform multimodal/complicated locomotion; third, excellent flexibility and stretchability to fit the unstructured environments.[10–14]

Historically, HMSMS has been widely employed in untethered soft robots,[6,7,9,11,15] active origami and metamaterials,[16–19] programmable and reconfigurable surfaces,[20–23] soft and flexible electronic devices,[24–27] targeted drug delivery,[3,28–33] etc. These applications generally take advantage of shape morphing of HMSMS, including bending,[9,33–37] folding,[16,18] and twisting.[19,38] What's more, the shape morphing behaviors of HMSMS under incompressible conditions have been systematically explored from both experimental and theoretical perspectives.[15,39–44] However, the application potential of volume deformation for HMSMS, for example, contraction deformation, has been overlooked. An HMSMS having both shape morphing and contraction deformation functions may be more valuable in some interesting fields, such as drug delivery. Factually, it is not easy for HMSMS to produce volume deformation since the elastomer or other soft materials used in HMSMS are often considered to be mechanically incompressible,[34,40] that is, no volume change during compression. By contrast, porous structures may offer an approach to realizing volume variation.[45] By introducing porous structures, the elastomer itself (i.e., Ecoflex-0030) is still an incompressible material while the structure of HMSMS can be compressed to realize volume deformation.

Inspired by porous structures, we reported anisotropic contraction with an ultra-soft hard magnetic foam (HMF) by dispersing neodymium–iron–boron (NdFeB) particles into an Ecoflex-0030 silicone matrix (**Figure 1**a), and following a sacrificial sugar cube template casting (Figure S1, Supporting Information). Ecoflex-0030 is chosen to be a deformable host to accommodate hard magnetic particles (NdFeB) due to its high stretchability (>400%), low elastic modulus (≈100 kPa), low viscosity, and simple fabrication process. As a result, the HMF is magnetically hard (with a residual magnetic flux density of

Z. Zong, S. Zhang, Z. Wu
State Key Laboratory of Digital Manufacturing Equipment and Technology
School of Mechanical Science and Technology
Huazhong University of Science and Technology
Wuhan 430074, China
E-mail: zhigang.wu@angstrom.uu.se

The ORCID identification number(s) for the author(s) of this article can be found under https://doi.org/10.1002/admt.202201255.
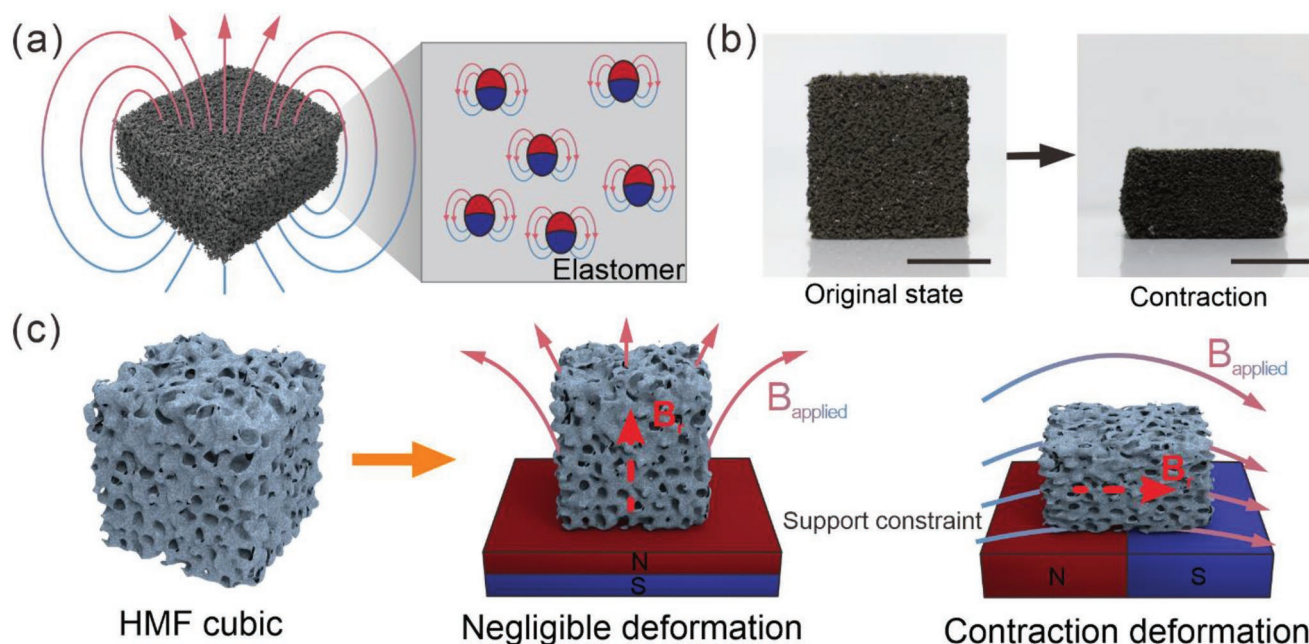
Figure 1. Anisotropic contraction of hard magnetic foam. a) Micro-CT reconfigured image of HMF. Inset: a sketch of the internal structure showing micromagnets (red and blue spheres) dispersed in a silicone elastomer matrix. b) Photographs of the original state and contraction state of HMF. Scale bar = 10 mm. c) Deformation of HMF in different magnetic fields.

12 mT) yet mechanically ultra-soft (with a shear modulus of 4.5 kPa). Of particular, we explored the mechanism of HMF's anisotropic contraction deformation and it majorly relates the following two factors: the elongation caused by magnetodeformational effect along the applied magnetic field directions, and the compression induced by the magnetic body-forces with a support constraint toward the magnet. By tuning the relationship (synergy or antagonism) between the two factors, the HMF bulk can undergo obvious contraction or negligible deformation, and by regulating the elastic modulus, porosity, and NdFeB contents of HMF, the contraction deformation degree could be adjusted from 0% to 43% (Figure 1b,c). Finally, the anisotropic contraction and flexible locomotion abilities under magnetic fields were utilized to realize precision drug delivery. Compared with the previous works,[31–33,46,47] our demonstrated HMF-based drug delivery soft robot could simultaneously achieve no leakage during moving, precisely adjustable drug release rate (from 0.008 to 0.62 mL min^{-1}, a 78 times span increase), and no drug residues after leaving.

2. Results and Discussion

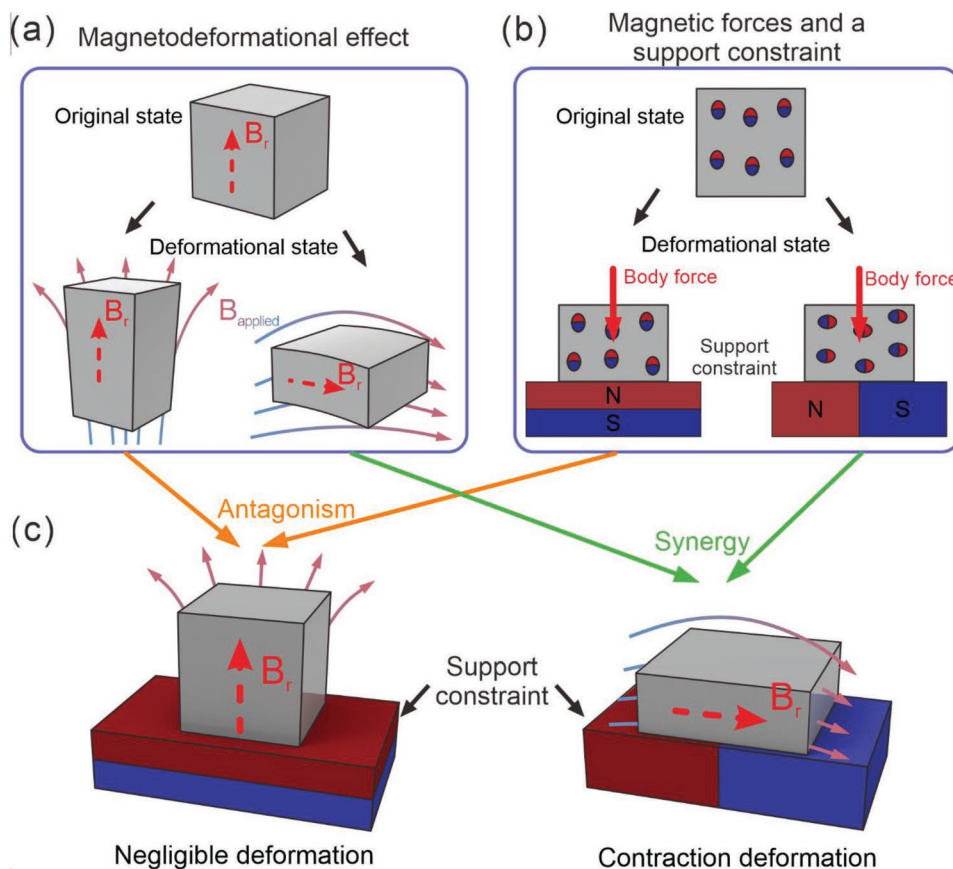### 2.1. Mechanisms of HMF's Anisotropic Contraction Deformation

As mentioned earlier, the anisotropic contraction deformation is majorly derived from two parts: one is the elongation along the applied magnetic field induced by magnetodeformational effect; the other is the compression caused by magnetic body force against a support constraint. We will analyze one by one HMF's deformation based on the above two issues.

Regarding the first issue, magnetic soft composites undergo shape deformation in applied magnetic fields.[4,14,41,48,49] When the applied magnetic field's direction and the HMF's remanence direction are aligned, the HMF will elongate along the applied field's direction; conversely, when the applied magnetic field's direction is opposite to the HMF's remanence direction, the HMF will contract along the applied field's direction. In external spatially homogeneous magnetic fields, this phenomenon is called the magnetostriction effect[50,51] (Figure S2, Supporting Information); while in non-uniform magnetic fields, this phenomenon is called magnetodeformational effect (**Figure** 2a).[52–57] In our work, the applied magnetic field to HMF bulk is derived from a permanent magnet below and thus the applied magnetic field is non-uniform, that is, only the magnetodeformational effect exists.

However, the deformation degree caused by the magnetodeformational effect is difficult to calculate since the non-uniform magnetic field is complicated and our HMF bulk isn't a mass point. Therefore, to digitally demonstrate how much deformation induced by magneto-deformational effect the HMF will undergo, we assume that the applied magnetic field where the HMF is exposed is uniform since the HMF bulk is so small compared to the volume of the magnet below. Previously, Zhao et al.[40] reported that the deformation of HMSMS in an applied uniform magnetic field could be expressed by

$$\lambda - \frac{1}{\lambda^2} = \frac{1}{\mu_0 G} B_r \cdot B_{applied} \tag{1}$$

where λ is the ratio of deformed length to the original length along the applied magnetic field directions, μ_0 refers to the vacuum permittivity, G refers to the shear modulus, B_r refers to the residual magnetic flux density of HMF, and

Figure 2. Mechanisms of HMF's anisotropic contraction. a) Magnetodeformational effect of HMF in an applied non-uniform magnetic field. b) Compression of HMF induced by the magnetic forces from the magnet below and a support constraint. c) Anisotropic response of HMF in different magnetic fields.

$B_{applied}$ refers to the applied magnetic flux density. Obviously, the deformation is directly related to the shear modulus and residual magnetic flux density of HMF. Therefore, to enhance the degree of deformation, a material with low shear modulus and high remanence is highly demanded. For HMF with 15 g NdFeB particles, the λ is 22% when the applied magnetic field is 250 mT.
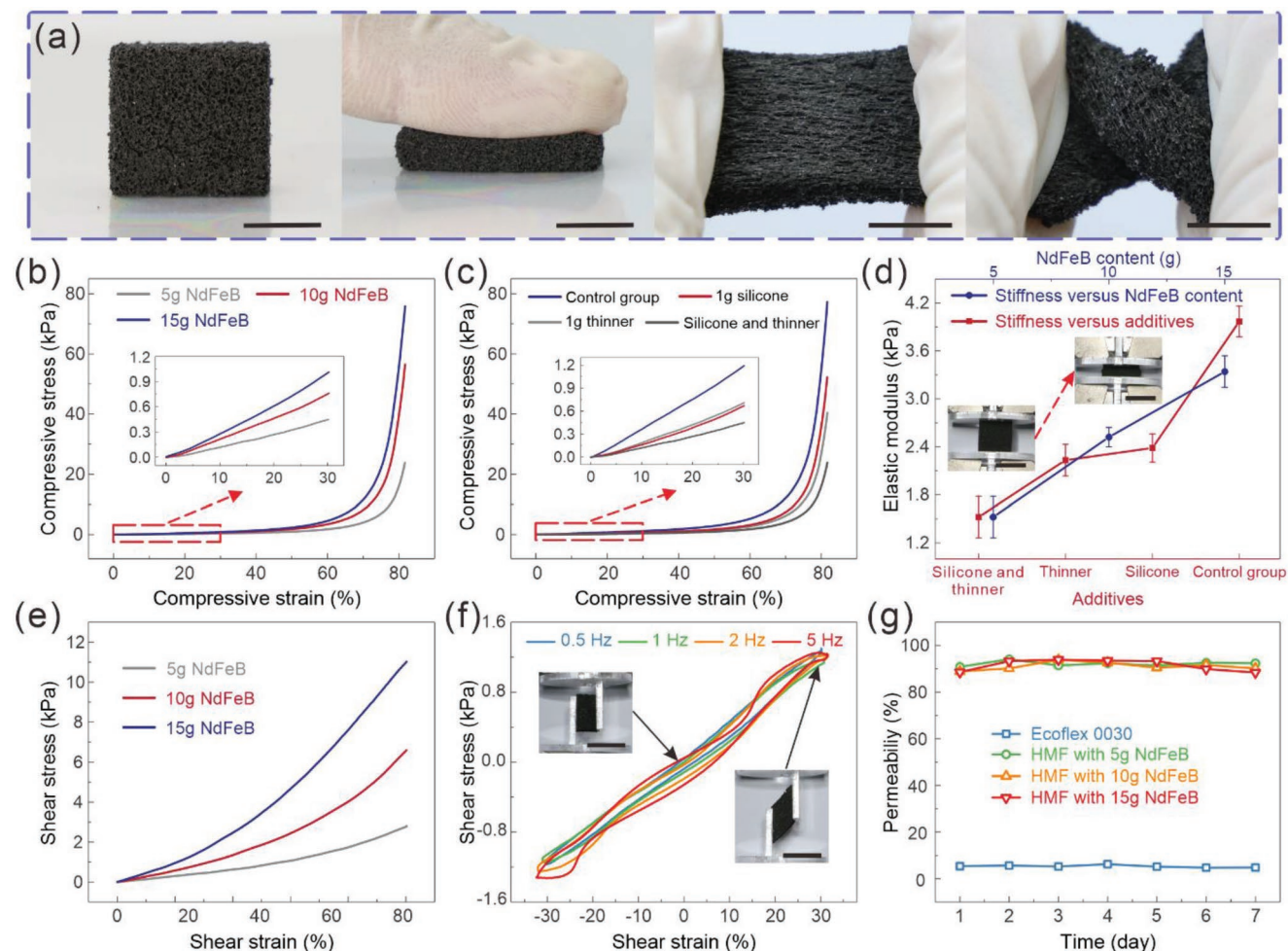
Simultaneously, regarding the second issue, a non-uniform applied magnetic field applies magnetic forces and torques to the magnetic soft composites. When the applied magnetic field is not aligned with the remanence direction of HMF, magnetic micro-torques are generated to rotate the HMF so that the HMF's remanence direction tends to align with the applied magnetic field.[1,58,59] Consequently, when the HMF is placed on a magnet, as depicted in Figure 2b, only these two scenarios can remain stable. In both cases, the HMF is subjected to a magnetic body force from the magnet below and then under a support constraint, the magnetic forces will cause compression of HMF bulks.

Since the Poisson's ratio is about 0.49, silicone elastomer (Ecoflex-0030) is considered to be incompressible[40] in continuum mechanics and the theory of elasticity. After utilizing a porous structure, many cavities are introduced into the HMF. When the HMF bulk is compressed, the air in the HMF's cavities escapes. Finally, the porous structure is compressed

into a solid to realize a volume change in HMF bulk. Therefore, after magnetization, HMF has isotropic mechanical properties and an anisotropic magnetic response. As schematically illustrated in Figure 2c, when the magnet is placed as the left half, the elongation caused by the magnetodeformational effect and the compression induced by the magnetic body forces act antagonistically to each other in the vertical direction, thus, there is no significant change in HMF's volume; while in the right half of Figure 2c, the compression caused by the magnetodeformational effect and the compression induced by the magnetic body forces act synergically in the vertical direction, contributing to large volume contraction. Consequently, an anisotropic contraction deformation is achieved.

Being a porous structure, it is assumed that the HMF bulk can be divided into many cells and each cell has its own remanence direction and will be subject to a magnetic micro-force/torque. The cells close to the magnet are subject to a greater magnetic micro-force and the cells above will compress the cells below due to their own downward magnetic micro-force. Therefore, the part of HMF close to the magnet below is deformed to a large degree and has high stiffness, which approximates solids. Furthermore, in the contraction state, the HMF not only contracts vertically but also elongates transversely (within about 5%).

**ADVANCED
SCIENCE NEWS**

www.advancedsciencenews.com

**ADVANCED
MATERIALS
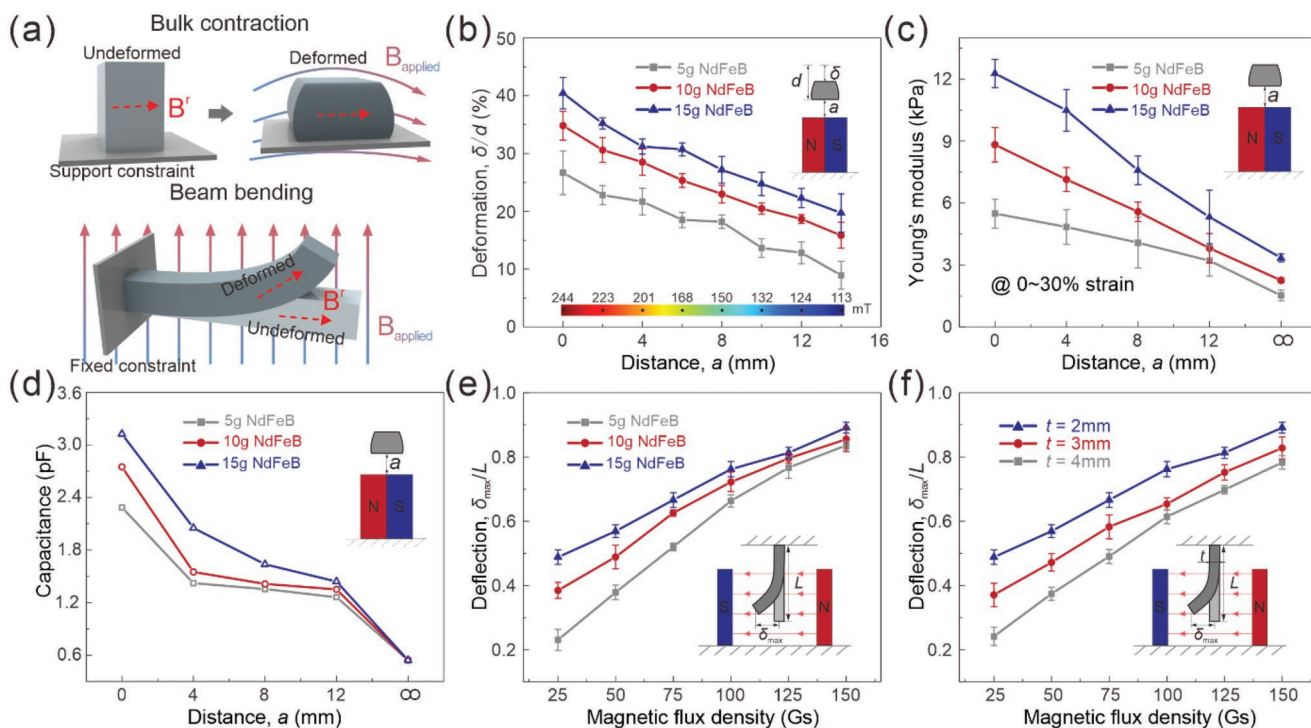TECHNOLOGIES**

www.advmattechnol.de

Figure 3. Mechanical properties of HMF. a) Images of the HMF in original, compressing, stretching, and twisting state. Scale bar = 10 mm. Compressive stress–strain curves for HMF with various amounts of b) NdFeB contents and c) additives. Inset indicates the compressive stress–strain curves in the linear region (0–30% strain). d) The elastic modulus fitted by linear region under various NdFeB and additive conditions. Inset indicates measurement setup. Scale bar = 20 mm. e) Static shear stress–strain curves for HMF with NdFeB contents of 5, 10, and 15 g. f) The HMF dynamic shear stress–strain curves. Inset indicates measurement setup. Scale bar = 20 mm. g) Air permeability experiments conducted for 8 days.

2.2. Mechanical Performances of HMF

Our HMF is ultra-soft and compliant due to its high-porosity 3D porous structure (**Figure 3**). We investigated the internal architecture of HMF using micro-computed tomography (micro-CT) tomography, complemented with a stereoscopic microscope recorded the external surface and cross-sectional viewpoints of HMF (Figure S3, Supporting Information). The pores in HMF are dispersed isotropically, as in Figures S3 and S4, Supporting Information, which contributes to the isotropic mechanical performances.

Figure 3a illustrates that our HMF could be easily compressed almost 80% by volume. HMF may also rapidly return to its initial state after being stretched and twisted to a great extent. Compressive stress versus strain curves of HMF with NdFeB contents of 5, 10, and 15 g are in Figure 3b, and they illustrate how the NdFeB particles affect the mechanical performance of HMF. The curves of 0–30% strain show good linearity, which indicates the isotropic porous structure.

The compressive strain–stress curves of HMF with various additives are in Figure 3c. Simultaneously, the linear region of strain–stress curves fits Young's modulus illustrated in Figure 3d. The additives can reduce stiffness, and NdFeB particles in HMF can enhance residual magnetic flux density and stiffness. Concurrently, the additives can also reduce the curing rate and viscosity of Ecoflex, which allows for better infiltration of liquids into the pores of HMF. Figure 3e displays the static shear stress versus strain curves for HMF with various NdFeB contents. HMF has an extremely low static shear modulus owing to its high porosity. For HMF with 5 g NdFeB particles, an 80% shear strain can be obtained with only a 2.7 kPa shear force, while the conventional HMS-MS's shear modulus is several hundred kPa or more.[1,5] The dynamic shear strain–stress curves for HMF in Figure 3f exhibit viscoelasticity. Common materials with low elastic and shear modulus, for example, hydrogels, tend to have a high viscosity. However, HMF demonstrates low viscosity and high elasticity, resulting in a quick response (58 ms) during

**ADVANCED
SCIENCE NEWS**

www.advancedsciencenews.com

**ADVANCED
MATERIALS
TECHNOLOGIES**

www.advmattechnol.de

Figure 4. Deformation and characterization of HMF under various magnetic fields. a) Deformation of HMF bulk under two magnetic fields. Dotted lines and solid lines separately represent the magnetic induction lines of HMF bulk and applied magnetic field. b) Deformation of bulk contraction versus magnetic flux density with different NdFeB contents. c) Young's modulus variation versus magnetic flux density. Young's modulus was fitted by 0–30% strain. d) Capacitance variation of tactile sensor versus magnetic flux density. Deflection of HMF beam versus magnetic flux density with e) NdFeB contents and f) beam thickness.

compression-release cycles, as shown in Figure S5, Supporting Information.

Additionally, the final form of HMF is a negative replica of the sugar cubes. Due to the small size and high density of particles in sugar cubes, fabricated HMF has the characteristics of high porosity. As the sugar cubes are interconnected internally, the pores of HMF are also interconnected, contributing to good gas permeability as in Figure 3g and Figure S6, Supporting Information.

### 2.3. Deformation and Sensing Performances of HMF

As schematically illustrated in **Figure 4**a, when the HMF bulk is placed in a gradient (non-uniform) applied magnetic field, the HMF bulk will undergo contraction deformation under the conditions of a support constraint. When the applied magnetic field is not aligned with the direction of residual magnetic flux density of HMF, the HMF beam will show elastic bending deformation if there are local constraints such as a fixed end as shown in Figure 4a.[1,40]

To characterize the contraction deformation of HMF, an HMF bulk was placed on the top of a permanent magnet at a distance of a (Figure 4b). The original height of HMF bulk is d and the deformation is δ. We define δ/d as the deformation degree. As the distance a rises, the applied magnetic field will drop (exactly as the calibration scalar in Figure 4b), and consequently the deformation decrease. Moreover, the NdFeB

contents can visibly alter the deformation of HMF bulk. The deformation of HMF with 15 g NdFeB is 65% greater than that of HMF with 5 g NdFeB.

With the same experimental setup, we measured Young's modulus (Figure 4c) based on the 0–30% strain region and the initial capacitance value of HMF. When the HMF bulk is placed into a non-uniform magnetic field (just like that in Figure 4a), the contraction deformation degree of HMF is non-homogeneous. The magnetic force (body force) induced by the magnet below acts throughout the volume of an HMF bulk. Young's modulus and initial capacitance all significantly increase as a result of the contraction of HMF; for instance, Young's modulus of HMF with 15 g NdFeB in a magnetic field is up to four times more than that without a magnetic field (Figure S7, Supporting Information). Additionally, as demonstrated in Figure S8, Supporting Information, the applied magnetic field can significantly alter the detecting signals of tactile sensors.

As demonstrated in Figure 4e,f, when one end of the HMF beam is fixed, the elastic deflection will take place under the applied magnetic field. HMF has a maximum deflection δ_{max} and an initial length of L. We define δ_{max}/L as the deflection degree of HMF. Greater deflection degree is caused by increased applied magnetic flux density, increased NdFeB concentration, and decreased HMF thickness. Of particular, due to the ultra-soft porous structures, the HMF can be actuated to realize rolling locomotion under a low actuating magnetic field, which can be actuated by a 100 Gs magnetic field to reach 80% deflection of its original length.
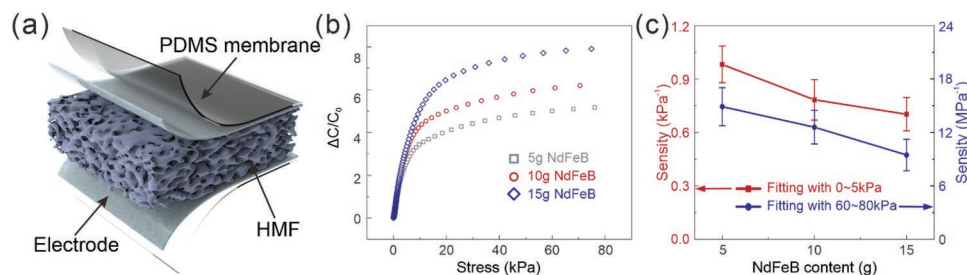
Figure 5. Electrical characterizations of a tactile sensor made of HMF. a) Schematic diagram of HMF-based capacitive tactile sensor with a square area of 4 cm² and an initial thickness of 10 mm. b) Comparison of capacitance variation versus the stress of tactile sensor with various NdFeB contents. c) Sensitivities fitted by two regions of a tactile sensor with various NdFeB contents.

Additionally, as a porous medium, HMF also can serve as a functional part of a tactile sensor[60,61] (**Figure 5**). As in Figure 5a, the tactile sensor is fabricated using a sandwich structure. We used a conductive fabric as the electrode and a 200 µm PDMS (20:1) membrane as an electrode substrate. As in Figure S9, Supporting Information, we used an LCR meter and a dielectric fixture to evaluate the permittivity of HMF. HMF's permittivity can be raised by NdFeB particles, and the effects of additives on permittivity are minimal. Furthermore, the permittivity of HMF cannot be impacted by the applied magnetic field. The sensitivity of a capacitive tactile sensor is defined as $S = \delta(\Delta C/C_0)/\delta P$, where C and C_0 stand for the capacitance that was measured and the capacitance that existed before applying pressure (P).[62–64] The sensitivity of tactile sensors with various parameters is shown in Figure 5b,c. The stiffness and permittivity can both greatly increase with the increase of the NdFeB particles. Higher permittivity variation under compression and lower media stiffness results in higher sensitivity for capacitance tactile sensors. Furthermore, the reliable input–output relation is played by strong mechanical durability under long-term or cyclic use. The sensors show nearly no signal drift or variation after 20 000 cycles of repeated compression-release tests (Figure S5, Supporting Information).

2.4. Application Demonstration

Currently, modern medicine, especially so-called precision medicine primarily relies on the use of drugs to manage and treat diseases. Thus, drug delivery is a critical field in medicine and healthcare.[65,66] In many scenarios, controlled drug delivery is required to deliver drugs to the target organ and then control the drug release rate to maintain a proper therapeutic concentration. Magnetic soft robots have been developed as a preferable strategy for in vivo drug delivery because of their untethered manipulation.[9,47,67–69] Moreover, the porous media is also an ideal carrier for medicines.[45,70–72]

Based on the anisotropic contraction deformation and flexible locomotion abilities of HMF in an applied specific magnetic field, an HMF-based drug delivery soft robot for the stomach was fabricated and the schematic illustration was shown in **Figure 6**a,b. The drug delivery robot carrying "drugs" rolled to the "tumor" under the control of an applied magnetic field generated by a permanent magnet. After the robots have moved

to the destination locations, the HMF bulk was controlled to contract under a specific magnetic field. The Figure 6b depicts two locomotion states of HMF-based drug delivery soft robots. Thin copper wires were attached to the two ends of HMF to output the electrical signal. In the future in vivo experiments, HMF-based drug delivery soft robots with a soft signal acquisition module and a Bluetooth module will be investigated. Drugs flowed out during the compression process and were absorbed by the absorbent paper. In Figure 6c,f, a drug delivery robot was controlled to carry drugs and release them in three places (Video S1, Supporting Information). By controlling the spatial locations and applied time of the permanent magnet, the drug was released at each of the three target locations in predesigned doses. It was noted that the applied magnetic field was only 100 Gs during the rolling locomotion of drug delivery soft robots, which would not cause obvious harm to creatures and environments.

Benefiting from the anisotropic contraction and flexible rolling locomotion abilities, HMF-based soft robots can realize precise drug delivery owing to the following features. First, from the aspect of drug release rate control/regulation, it increases from 0.008 to 0.62 mL min⁻¹ precisely, reaching a 78 times span increase under the applied magnetic field (Figure 6d). Second, from the aspect of temporal response control of drug release, once the applied magnetic field was removed, the HMF bulk would elongate and recover to the original state immediately. The recovery of HMF would reabsorb the drug that has not yet been absorbed by tissues into HMF bulk (Figure 6e and Figure S10 and Video S2, Supporting Information). Third, from the aspect of leakage prevention of drug during moving, the contraction deformation and bending deformation of HMF are independent since the anisotropic contraction occurs in the steady state while the rolling locomotion occurs in the dynamic state and the applied magnetic field to actuate locomotion of HMF is just one-twentieth, or perhaps less, of the magnetic field that causes it to contract. Hence, it is not necessary to worry that the HMF-based soft robots show drug leakage due to contraction deformation during rolling locomotion. Furthermore, in future in vivo practice, some auxiliary tools, such as computer tomography, magnetic resonance imaging, and 3D ultrasound imaging, can be used to realize more precise drug delivery. These tools can help visualize the environment circumstance of stomach's tumor and with them, we could tune the strength and orientations of the magnetic field to eliminate
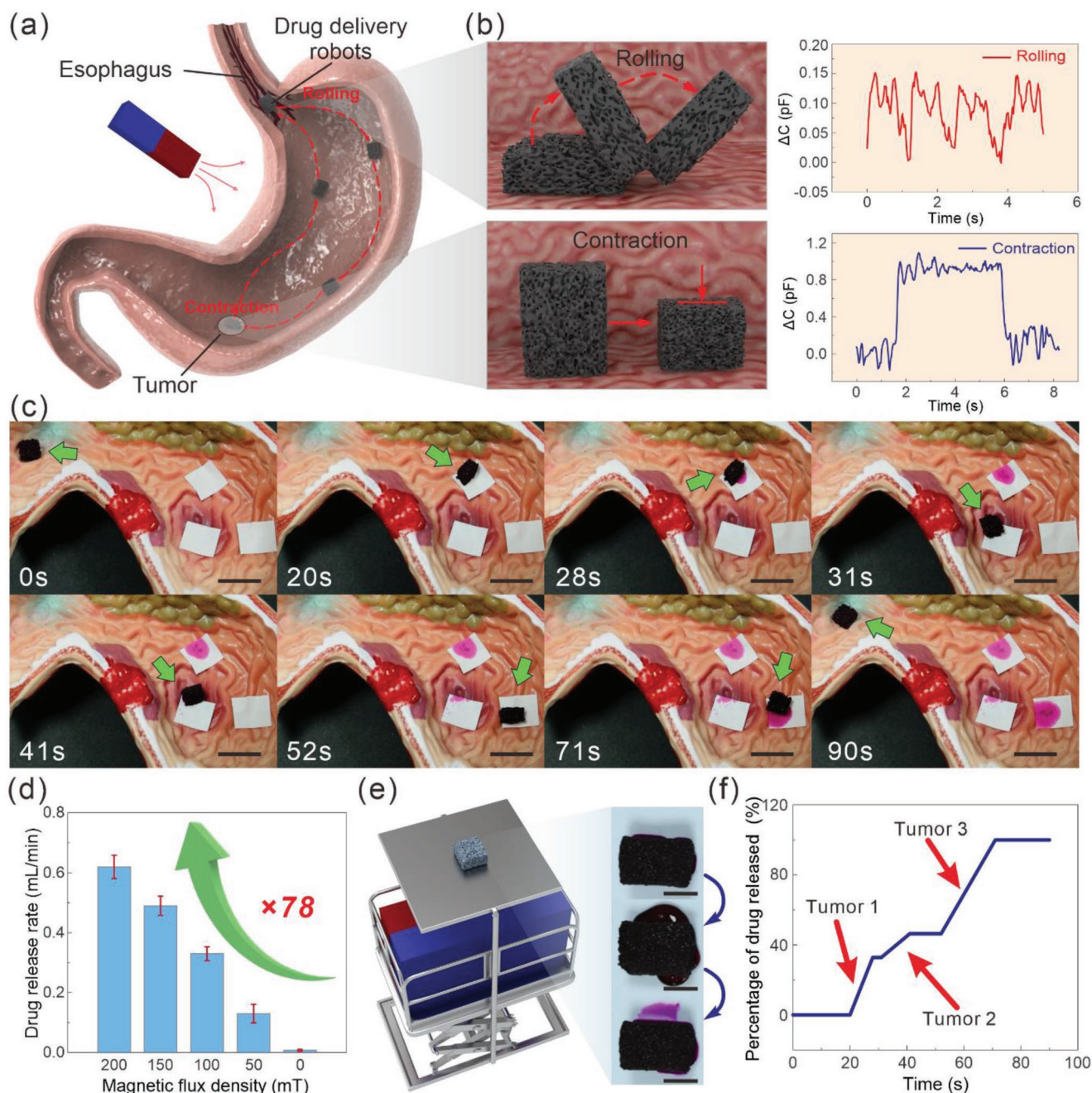
Figure 6. Magnetically actuated soft HMF robots for drug delivery. a) Application scenario. The robot reached a tumor with rolling locomotion. Afterward, the robot released drugs stored in its body by contraction and then returned to start. b) Rolling locomotion and contraction of drug delivery robot and corresponding sensing signal. c) Sequential images of drug delivery by HMF robot. Scale bar = 5 mm. d) Drug release rate versus applied magnetic flux density. e) Progress of drug release and reabsorption. Scale bar = 10 mm. f) Percentage of drug released versus time in the drug release process.

the difference of flat layer and muscle layer between each person's body.

In brief, a $5 \times 5 \times 3$ mm^3 HMF bulk was used to be a precision drug delivery soft robot. Compared with the previous works, besides more precise drug releasing, the robots had the advantages of small size, low actuating magnetic field, large carrying capacity, high reliability, and good sensing capability at the same time, as shown in **Table 1**.

3. Conclusion

We fabricated a mechanically ultra-soft but magnetically hard porous structure, HMF, by dispersing high-coercivity ferromagnetic particles into a soft silicone matrix. We observed an anisotropic contraction in HMF and explored its mechanism behind. Such an anisotropic contraction deformation arises from the magnetodeformational effect and magnetic body-force

**ADVANCED
SCIENCE NEWS**

www.advancedsciencenews.com

**ADVANCED
MATERIALS
TECHNOLOGIES**

www.advmattechnol.de

Table 1. Comparison of the performance of the reported drug delivery robots.

Drug delivery robot	Applied magnetic field [mT]	Volume/Mass	Sensing strategy	Reliability	Carrying capacity
[30]	—	Diameter: 6–≈8 µm	No	Low	High
[45]	—	Diameter: 11 mm, Height: 8 mm	No	Low	High
[31]	<1400	Length: 30 mm Mass: 8 g	No	High	Low
[32]	<50	Diameter: 4.5 mm, Height: 2 mm	No	Low	High
[73]	<100	$20 \times 5 \times 3$ mm^3	No	Low	High
[33]	<400	$40 \times 5 \times 2$ mm^3	No	High	Low
[47]	<1200	Diameter: 10 mm, Height: 30 mm	Vision	High	Low
Current work	<10	$5 \times 5 \times 3$ mm^3	Tactile sensing	High	High

against the support constraint: when the above two factors act synergically, the HMF contracts; when they act antagonistically, there is no significant deformation in HMF. Benefiting from the introduction of porous structures and high coercivity NdFeB particles, the HMF has both flexible rolling locomotion and contraction abilities, which well matches the demands of precision drug delivery. Furthermore, precise control under magnetic field and reabsorption abilities of HMF achieve adjustable drug release rate, precise location drug release, and no residues after leaving.

4. Experimental Section

Fabrication Process of HMF Bulk: 5 g ferromagnetic particles (MQFB-B-20076-089, Magnequench, USA) and 5 g A part of Ecoflex-0030 (Smooth-On, USA) were mixed by a mixing defoamer (ARE-310, Thinky, Japan, 800 rpm for 1 min, 1200 rpm for 30 s, 1600 rpm for 1 min, and 1800 rpm for 30 s), and then mixed with 5 g B part of Ecoflex-0030. 1 or 2 g additives, silicone oil, or Ecoflex thinner, were poured into the mixture and mixed well. Then, the uncured solution was poured equally into three molds fabricated by 3D printing (E3, Hori, China) with a size of $25 \times 25 \times 20$ mm^3. A sugar cube (cube sugar, Taikoo, China) was placed into a mold and vacuumed for 20 min. Then the molds were placed at 4 °C for 12 h. The sugar cubes were taken out of the molds and any extra Ecoflex-0030 was wiped off from their surfaces. Finally, the sugar cubes were heated in an oven (UF 55 plus, Memmert, Germany) at 70 °C for 2 h before being immersed in water to dissolve the sacrificial sugar template. The water was heated to 80 °C and mixed for 1 h on a magnetic mixer (HS 7, IKA, Germany). After thoroughly dissolving the sacrificial sugar templates, the HMF bulks were removed and dried at 50 °C for 30 min or at room temperature for 5 h. A capacitive high-voltage magnetizer (MAG-3000, CH-Magnetoelectricity Technology, China) was used to magnetize the prepared HMF bulk.

Characterizations of HMF Bulk: The profile and cross section of HMF were observed using a stereoscopic microscope (Stemi 508, Carl Zeiss, Germany). The detailed pores distribution of HMF was reconfigured using micro-CT (SkyScan 1176, BRUKER, Germany). The microstructure of the cross section was examined using scanning electron microscope (SU3900, Hitachi, Japan). A digital camera (EOS 70D, Canon, Japan) was used to record the macro deformation of HMF bulk by hand. The compression test was conducted with a universal testing system (5944, Instron, USA). The dynamic shear test was conducted with a dynamic testing instrument (E1000, Instron, USA). A precision LCR meter (E4980AL, Keysight Technologies, USA) connected to a dielectric fixture (16451B, Keysight Technologies, USA) was used to measure the capacitance and dielectric permittivity of tactile sensors.

Fabrication of Tactile Sensor with HMF: A 200 µm PDMS (10:1) flexible film was applied to a polyethylene terephthalate (PET) substrate (YH-2910, Yuanhao, China) with an automatic coating machine (ZAA 2300, ZEHNTNER, Switzerland). The conductive fabric electrodes (from Alibaba, China) were cut into desired shapes by a UV laser marker system (HGL-LSU3/5EI, Huagong Laser, China) and placed on the PDMS film. PDMS film and conductive fabric were removed from the PET substrate. The HMF bulk was assembled to the conductive fabric electrodes by adhesive rubber (Silpoxy, Smooth-on, USA). The copper wires were attached to the electrodes using conductive Ag paste (from Alibaba, China).

Deformation Characterization of HMF: An HMF bulk was positioned on top of a permanent magnet (N52, Alibaba, China) or in the center of two permanent magnets. The distance between the HMF bulk and the permanent magnet was adjusted using 1 mm slides. The deformation of HMF bulk was recorded using a digital camera (EOS R5, Canon, Japan). ImageJ was used to calculate the precise deformation amount from the pictures.

Demonstration of Drug Delivery: The HMF bulk was cut into a $5 \times 5 \times 3$ mm^3 piece and then injected with distilled water dyed with rhodamine B (Aladdin, Shanghai, China). A polyvinyl chloride model stomach ($160 \times 110 \times 55$ mm^3, from Alibaba, China) was used to mimic the stomach environment. The absorbent paper (from JD.COM, China) attached to the stomach model was used to absorb the dyed distilled water. The permanent magnet ($300 \times 200 \times 150$ mm^3, from Alibaba, China) was used to control the locomotion and contraction of HMF-based soft robots.

Statistical Analysis: For statistical analysis, samples were tested in $n \geq 3$ replicates and all the data were expressed as mean ± standard error. The least squares method was utilized to count data. MATLAB R2020b was used to process data.

Supporting Information

Supporting Information is available from the Wiley Online Library or from the author.

Acknowledgements

Conflict of Interest

The authors declare no conflict of interest.

Data Availability Statement

The data that support the findings of this study are available in the supplementary material of this article.

Keywords

anisotropic contraction, drug deliveries, hard magnetic foams, low actuating magnetic fields, magnetodeformational effects, porous structures, shape morphing

[1] S. Wu, W. Hu, Q. Ze, M. Sitti, R. Zhao, *Multifunct. Mater.* **2020**, *3*, 042003.

[2] D. Garcia-Gonzalez, *Smart Mater. Struct.* **2019**, *28*, 085020.

[3] H. Li, G. Go, S. Y. Ko, J. O. Park, S. Park, *SmartMater. Struct.* **2016**, *25*, 027001.

[4] Z. Shen, F. Chen, X. Zhu, K. T. Yong, G. Gu, *J. Mater. Chem. B* **2020**, *8*, 8972.

[5] Y. Kim, X. Zhao, *Chem. Rev.* **2022**, *122*, 5317.

[6] E. Diller, J. Zhuang, G. Z. Lum, M. R. Edwards, M. Sitti, *Appl. Phys. Lett.* **2014**, *104*, 174101.

[7] G. Z. Lum, Z. Ye, X. Dong, H. Marvi, O. Erin, W. Hu, M. Sitti, *Proc. Natl. Acad. Sci. USA* **2016**, *113*, E6007.

[8] N. El-Atab, R. B. Mishra, F. Al-Modaf, L. Joharji, A. A. Alsharif, H. Alamoudi, M. Diaz, N. Qaiser, M. M. Hussain, *Adv. Intell. Syst.* **2020**, *2*, 2000128.

[9] X. Ke, S. Zhang, Z. Chai, J. Jiang, Y. Xu, B. Tao, H. Ding, Z. Wu, *Mater. Today Phys.* **2021**, *17*, 100313.

[10] J. M. D. Coey, *IEEE Trans. Magn.* **2011**, *47*, 4671.

[11] E. Y. Kramarenko, A. V. Chertovich, G. V. Stepanov, A. S. Semisalova, L. A. Makarova, N. S. Perov, A. R. Khokhlov, *Smart Mater. Struct.* **2015**, *24*, 035002.

[12] G. V. Stepanov, D. Y. Borin, P. A. Storozhenko, *J. Magn. Magn. Mater.* **2017**, *431*, 138.

[13] L. Wang, Y. Kim, C. F. Guo, X. Zhao, *J. Mech. Phys. Solids* **2020**, *142*, 104045.

[14] S. Lucarini, M. Hossain, D. Garcia-Gonzalez, *Compos. Struct.* **2022**, *279*, 114800.

[15] Z. Ren, W. Hu, X. Dong, M. Sitti, *Nat. Commun.* **2019**, *10*, 2703.

[16] H. Song, H. Lee, J. Lee, J. K. Choe, S. Lee, J. Y. Yi, S. Park, J. W. Yoo, M. S. Kwon, J. Kim, *Nano Lett.* **2020**, *20*, 5185.

[17] J. Cui, T. Y. Huang, Z. Luo, P. Testa, H. Gu, X. Z. Chen, B. J. Nelson, L. J. Heyderman, *Nature* **2019**, *575*, 164.

[18] L. Bowen, K. Springsteen, H. Feldstein, M. Frecker, T. W. Simpson, P. von Lockette, *J. Mech. Robot.* **2015**, *7*, 011010.

[19] J. Zhang, Z. Ren, W. Hu, R. H. Soon, I. C. Yasa, Z. Liu, M. Sitti, *Sci. Robot.* **2021**, *6*, eabf0112.

[20] Z. Wang, K. Wang, D. Liang, L. Yan, K. Ni, H. Huang, B. Li, Z. Guo, J. Wang, X. Ma, X. Tang, L. Q. Chen, *Adv. Mater.* **2020**, *32*, 2001879.

[21] Z. Yang, J. K. Park, S. Kim, *Small* **2018**, *14*, 1702839.

[22] Y. Lin, Z. Hu, M. Zhang, T. Xu, S. Feng, L. Jiang, Y. Zheng, *Adv. Funct. Mater.* **2018**, *28*, 1800163.

[23] D. M. Drotlef, P. Blümler, P. Papadopoulos, A. Del Campo, *ACS Appl. Mater. Interfaces* **2014**, *6*, 8702.

[24] Z. Qi, M. Zhou, Y. Li, Z. Xia, W. Huo, X. Huang, *Adv. Mater. Technol.* **2021**, *6*, 2001124.

[25] Y. Yan, Z. Hu, Z. Yang, W. Yuan, C. Song, J. Pan, Y. Shen, *Sci. Robot.* **2021**, *6*, 51.

[26] T. Hellebrekers, O. Kroemer, C. Majidi, *Adv. Intell. Syst.* **2019**, *1*, 1900025.

[27] Y. Wu, Y. Liu, Y. Zhou, Q. Man, C. Hu, W. Asghar, F. Li, Z. Yu, J. Shang, G. Liu, M. Liao, R. W. Li, *Sci. Robot.* **2018**, *3*, eaat0429.

[28] N. S. Satarkar, J. Z. Hilt, *J. Controlled Release* **2008**, *130*, 246.

[29] Z. Yang, H. Peng, W. Wang, T. Liu, *J. Appl. Polym. Sci.* **2010**, *116*, 2658.

[30] A. V. Singh, Z. Hosseinidoust, B. W. Park, O. Yasa, M. Sitti, *ACS Nano* **2017**, *11*, 9759.

[31] S. Yim, M. Sitti, *IEEE Trans. Robot.* **2012**, *28*, 183.

[32] S. Fusco, M. S. Sakar, S. Kennedy, C. Peters, R. Bottani, F. Starsich, A. Mao, G. A. Sotiriou, S. Pané, S. E. Pratsinis, D. Mooney, B. J. Nelson, *Adv. Mater.* **2014**, *26*, 952.

[33] E. B. Joyee, Y. Pan, *J. Manuf. Process.* **2020**, *56*, 1178.

[34] H. Ye, Y. Li, T. Zhang, *Soft Matter* **2021**, *17*, 3560.

[35] L. Zhang, G. Wu, J. Sun, B. Zi, W. Chen, Y. Wu, *ACS Nano* **2021**, *15*, 5294.

[36] X. Zhu, Y. Hu, G. Wu, W. Chen, N. Bao, *ACS Nano* **2021**, *15*, 9273.

[37] G. Wu, X. Wu, Y. Xu, H. Cheng, J. Meng, Q. Yu, X. Shi, K. Zhang, W. Chen, S. Chen, *Adv. Mater* **2019**, *31*, 1806492.

[38] C. Wu, Q. Zhang, X. Fan, Y. Song, Q. Zheng, *J. Intell. Mater. Syst. Struct.* **2019**, *30*, 1084.

[39] L. Liu, *J. Mech. Phys. Solids* **2014**, *63*, 451.

[40] R. Zhao, Y. Kim, S. A. Chester, P. Sharma, X. Zhao, *J. Mech. Phys. Solids* **2019**, *124*, 244.

[41] W. Chen, L. Wang, *J. Appl. Mech. Trans. ASME* **2020**, *87*, 041002.

[42] Z. Xing, H. Yong, *Int. J. Smart Nano Mater.* **2021**, *12*, 429.

[43] L. Chen, K. Tan, S. Yang, Q. Deng, *Int. J. Solids Struct.* **2022**, *246–247*, 111607.

[44] F. Dadgar-Rad, M. Hossain, *Int. J. Solids Struct.* **2022**, *251*, 111747.

[45] X. Zhao, J. Kim, C. A. Cezar, N. Huebsch, K. Lee, K. Bouhadir, D. J. Mooney, *Proc. Natl. Acad. Sci. USA* **2011**, *108*, 67.

[46] M. Cianchetti, C. Laschi, A. Menciassi, P. Dario, *Nat. Rev. Mater.* **2018**, *3*, 143.

[47] D. Son, H. Gilbert, M. Sitti, *Soft Robot.* **2020**, *7*, 10.

[48] W. Chen, Z. Yan, L. Wang, *Soft Matter* **2020**, *16*, 6379.

[49] R. Zhang, S. Wu, Q. Ze, R. Zhao, *J. Appl. Mech. Trans. ASME* **2020**, *87*, 091008.

[50] H. D. Chopra, M. Wuttig, *Nature* **2015**, *521*, 340.

[51] Y. Zhou, X. Zhao, J. Xu, Y. Fang, G. Chen, Y. Song, S. Li, J. Chen, *Nat. Mater.* **2021**, *20*, 1670.

[52] R. Patel, R. V. Upadhyay, R. V. Mehta, *J. Phys. Condens. Matter* **2008**, *20*, 204116.

[53] Y. L. Raikher, O. V. Stolbov, *J. Magn. Magn. Mater.* **2005**, *289*, 62.

[54] L. V. Nikitin, G. V. Stepanov, L. S. Mironova, A. I. Gorbunov, *J. Magn. Magn. Mater.* **2004**, *272–276*, 2072.

[55] G. V. Stepanov, D. Y. Borin, Y. L. Raikher, P. V. Melenev, N. S. Perov, *J. Phys. Condens. Matter* **2008**, *20*, 204121.

[56] G. V. Stepanov, E. Y. Kramarenko, D. A. Semerenko, *J. Phys. Conf. Ser.* **2013**, *412*, 012031.

[57] E. Dohmen, D. Borin, *SmartMater. Struct.* **2022**, *31*, 025016.

[58] R. Pease, *Nature* **1988**, *328*, 12.

[59] G. Long, F. Grandjean, *Supermagnets, Hard Magnetic Materials*, Springer, Ciocco, Italy **1991**.

[60] B. Park, Y. Jung, J. S. Ko, J. Park, *Polymers* **2021**, *13*, 824.

[61] M. Charara, W. Luo, M. C. Saha, Y. Liu, *Adv. Eng. Mater.* **2019**, *21*, 1801068.

[62] N. Bai, L. Wang, Q. Wang, J. Deng, Y. Wang, P. Lu, J. Huang, G. Li, Y. Zhang, J. Yang, K. Xie, X. Zhao, C. F. Guo, *Nat. Commun.* **2020**, *11*, 3.

[63] Q. Lin, J. Huang, J. Yang, Y. Huang, Y. Zhang, Y. Wang, J. Zhang, Y. Wang, L. Yuan, M. Cai, X. Hou, W. Zhang, Y. Zhou, S. G. Chen, C. F. Guo, *Adv. Healthcare Mater.* **2020**, *9*, 2001023.

[64] T. Zhao, T. Li, L. Chen, L. Yuan, X. Li, J. Zhang, *ACS Appl. Mater. Interfaces* **2019**, *11*, 29466.

[65] M. W. Tibbitt, J. E. Dahlman, R. Langer, *J. Am. Chem. Soc.* **2016**, *138*, 704.

[66] Y. Zhang, H. F. Chan, K. W. Leong, *Adv. Drug Delivery Rev.* **2013**, *65*, 104.

[67] R. Tan, X. Yang, H. Lu, L. Yang, T. Zhang, J. Miao, Y. Feng, Y. Shen, *Matter* **2022**, *5*, 1277.

[68] H. Lu, Y. Hong, Y. Yang, Z. Yang, Y. Shen, *Adv. Sci.* **2020**, *7*, 2000069.

[69] H. Lu, M. Zhang, Y. Yang, Q. Huang, T. Fukuda, Z. Wang, Y. Shen, *Nat. Commun.* **2018**, *9*, 3944.

[70] P. Sher, G. Ingavle, S. Ponrathnam, A. P. Pawar, *Microporous Mesoporous Mater.* **2007**, *102*, 290.

[71] H. Yang, L. Hao, N. Zhao, C. Du, Y. Wang, *CrystEngComm* **2013**, *15*, 5760.

[72] G. Ahuja, K. Pathak, *Indian J. Pharm. Sci.* **2009**, *71*, 599.

[73] J. C. Breger, C. Yoon, R. Xiao, H. R. Kwag, M. O. Wang, J. P. Fisher, T. D. Nguyen, D. H. Gracias, *ACS Appl. Mater. Interfaces* **2015**, *7*, 3398.